LIMNOLOGY and OCEANOGRAPHY

ASLO

Limnol. Oceanogr. 9999, 2024, 1–16

doi: 10.1002/lno.12773

Consistent prokaryotic successional dynamics across contrasting phytoplankton blooms

Markel Gómez-Letona,[1,2*] **Javier Arístegui**,[1*] **Ulf Riebesell**,[3] **Marta Sebastián**[1,4]

[1]Instituto de Oceanografía y Cambio Global, Universidad de Las Palmas de Gran Canaria (ULPGC), Las Palmas, Spain
[2]Instituto de Investigacións Mariñas (IIM), CSIC, Vigo, Spain
[3]Biological Oceanography, Marine Biogeochemistry, GEOMAR Helmholtz Centre for Ocean Research Kiel, Kiel, Germany
[4]Department of Marine Biology and Oceanography, Institut de Ciències del Mar (ICM), CSIC, Barcelona, Spain

Abstract

Heterotrophic prokaryotes play a vital role in organic matter cycling in the ocean and have been observed to undergo substrate-controlled successions during phytoplankton blooms. However, there is limited understanding of the succession patterns during blooms triggered by upwelling events of different characteristics. Here we simulated eight upwelling scenarios of varying intensity and duration (single vs. recurring pulses) by adding nutrient-rich mesopelagic waters into large-scale mesocosms containing oligotrophic surface waters from the subtropical North Atlantic. Over a monitoring period of nearly 6 weeks, we observed that phytoplankton blooms displayed diverging outcomes depending on the upwelling mode: treatments with single upwelling pulses presented a unique, short-lived bloom, whereas recurring upwelling resulted in blooms that were sustained over time. Prokaryotic abundances were positively related to upwelling intensity and presented three similar abundance cycles in all treatments, whereas heterotrophic activity differed between the two upwelling modes. The successional dynamics of free-living and particle-associated communities were consistent regardless of upwelling intensity and mode, with four or five prokaryotic assemblages sequentially proliferating during the experiment. Yet, some differences were observed in the taxa that formed the assemblages in both upwelling modes. Together, our results suggest that, despite differences in activity, prokaryotes seemed to be more influenced by processes taking place within the community than by phytoplankton bloom patterns, with similar succession dynamics even under widely distinct blooms. These findings can help advance our understanding on prokaryotic ecology and its relation to organic matter cycling across different upwelling scenarios.

Phytoplankton can form large blooms under favorable environmental conditions, a process that has been extensively studied both in the field and experimentally (e.g., Leblanc et al. 2016; Sundby et al. 2016; Taucher et al. 2018). During blooming episodes, these autotrophic microorganisms fix large amounts of inorganic carbon into organic matter through photosynthesis. Part of the newly fixed carbon is later released as dissolved organic compounds by phytoplankton exudation (Mühlenbruch et al. 2018), prokaryotic extracellular enzymatic activity (Balmonte et al. 2021) and, especially during bloom termination, through grazing (Saba et al. 2011) and viral lysis (Kuhlisch et al. 2022). Organic matter thus becomes accessible to prokaryotic organisms (bacteria and archaea), which in turn consume and metabolize it in a continuous transformative cycle (Azam and Malfatti 2007).

Prokaryotic communities, harboring a myriad of metabolic traits (Moran 2015), are often dominated by a small number of taxa at any given time. These communities are, however, far from stationary. Changes in environmental conditions, such as increases in organic matter concentration observed during phytoplankton blooms, prompt shifts in community structure and gene expression within microbial communities (Teeling et al. 2012; Needham and Fuhrman 2016; Pontiller et al. 2022). The composition of organic matter has also been suggested as one of the main factors driving the taxonomic and transcriptional successions of prokaryotes, as taxa tend to specialize in particular sets of compounds (Teeling et al. 2012;

*Correspondence: markel.gomez101@alu.ulpgc.es; javier.aristegui@ulpgc.es

Additional Supporting Information may be found in the online version of this article.

Author Contribution Statement: Conceptualization: MGL, MS, UR, and JA. Funding Acquisition: UR and JA. Investigation: MGL, JA, UR, and MS. Formal Analysis: MGL. Visualization: MGL. Supervision: MS and JA. Writing—Original Draft Preparation: MGL. Writing—Review & Editing: MGL, MS, JA, and UR.

Pontiller et al. 2022). The resulting microbial landscape during phytoplankton blooms is one in which resources are partitioned among different prokaryotic taxa during the consecutive stages of the blooming episode. Thus, tracking the evolution of standing stocks, activity and taxonomic composition of prokaryotic communities can help us advance our understanding of the ecology of prokaryotes and the cycling of organic matter during phytoplankton blooms in different oceanic environments.

Upwelling regions are of major relevance when studying prokaryotic community dynamics under phytoplankton blooms. As one of the most productive environments in the global ocean (Chavez and Messié 2009), the microbes that inhabit them play a disproportionately large role in the marine carbon cycle (Capone and Hutchins 2013). The intensity and temporal extent of upwelling (and, hence, the associated productivity) varies between and within systems: from short-term events to seasonal to year-round, with varying degrees of upwelling strength (Cropper et al. 2014; Desbiolles et al. 2014; Bode et al. 2019). Current conditions in upwelling systems could, however, face changes in future decades under climate change (Bograd et al. 2023), potentially altering phytoplankton bloom patterns and the associated prokaryotic successions.

Here we explored whether prokaryotic activity and successions diverge under varying phytoplankton bloom dynamics in distinct upwelling scenarios or, conversely, if shared patterns exist. Using large-scale mesocosms, we introduced nutrient-rich waters from the upper mesopelagic into oligotrophic surface waters, simulating combinations of upwelling intensity and duration (single pulse vs. recurring upwelling), for a total of eight upwelling scenarios. We studied the temporal dynamics in standing stocks, activity, and taxonomic composition of prokaryotic communities, hypothesizing that the successions of prokaryotes would vary across the different upwelling scenarios.

Materials and methods

Experimental setup and sampling

Nine large-scale mesocosms (Riebesell et al. 2013) were deployed in Gando Bay (27° 55′ 41″ N, 15° 21′ 55″ W, Gran Canaria, Canary Islands) during the autumn of 2018 as part of the Ocean artUp project. Mesocosms were filled with ambient oligotrophic water (mean ± sd volume = 43.775 ± 1.352 m^3) and deep water was collected off Gran Canaria from 330 and 280 m depth (on day −10 and 23, respectively) by pumping it into a 100 m^3 opaque collector bag lowered from a ship (Taucher et al. 2017), which was then moored next to the mesocosms. This deep water was added to the mesocosms (subtracting an equivalent volume from them) in two different modes (Table 1): a singular mode (*S*), consisting of a single deep-water addition (on day 4), and a recurring mode (*R*), in which consecutive deep-water additions were performed (on days 4, 8, 12, 16, 21, 24, 28, and 32). For each upwelling mode, four levels of intensity were simulated: Low, Medium, High, and Extreme, resulting in an intensity range of approximately 1.6–10.5 μmol L^{-1} in terms of nitrogen addition (as sum of all the net nitrogen inputs of each water replacement, Table 1). Equivalent intensity levels of the singular and recurring modes received similar total amounts of nutrients (Table 1), so that the response to the two modes of addition could be compared for the different intensities. No deep water was added to the control mesocosm. The deep water added to the mesocosms was intended to be sourced from a depth of 600 m, where nitrate concentrations are approximately 25 μmol L^{-1} (Llinás et al. 1997), but this was not possible after equipment loss due to adverse sea conditions. Hence, to attain the targeted macronutrient concentrations and maintain their stoichiometric ratios, nitrate, phosphate and silicate were added to the deep water bag before the first addition to the mesocosms, yielding concentrations of 25, 1.38, and 12.1 μmol L^{-1} of nitrate, phosphate, and silicate, respectively (Baumann et al. 2021). Nutrients in the deep water bag were periodically measured and adjusted to ensure concentrations were maintained. Dissolved organic carbon (DOC) concentration in the deep water was of ∼ 80 μmol L^{-1} at the time of the first addition, although it increased to ∼ 180 μmol L^{-1} before being restored to ∼ 60 μmol L^{-1} (similar to that found in the collection area [Santana-Falcón et al. 2017]) when deep water was renewed on day 23. Particulate organic carbon (POC) tended to range between 10 and 20 μmol L^{-1}. Prokaryotic abundances also ranged approximately from ∼ 2.8×10^5 to 4×10^6 cells L^{-1} before going back to ∼ 2.2×10^5 when the deep water was renewed on day 23. Yet, these increases did not have a noticeable effect on the mesocosms, as these variables (and related ones) did not increase immediately after water additions.

Mesocosms and ambient waters outside of the mesocosms (*Atlantic*) were regularly sampled over 39 d (every day at the beginning, every second day after day 11), during which integrated samples of the water column (0–13 m) were collected using depth-integrated water samplers (IWS, HYDRO-BIOS, Kiel). The deep water bag (*Deep*) was also sampled periodically to monitor it. Sampled water was dispensed into acid-cleaned canisters and kept in dark, cool conditions until returning to the lab.

Prokaryotic abundances and viability

Abundance of prokaryotic cells was quantified by flow cytometry. Samples were fixed with paraformaldehyde at a final concentration of 2% (v/v) and kept at −80°C until further processing. Samples were thawed and analyzed in a FACSCalibur flow cytometer (Becton-Dickinson), staining subsamples (400 μL) with 4 μL of the SYBR Green I fluorochrome (Molecular Probes) diluted in dimethyl sulfoxide (1:10). Fluorescent beads (1 μm, Polysciences) were added for internal calibration (10^5 mL^{-1}). High and low nucleic acid content (HNA and LNA, respectively) prokaryotic cells were identified in green vs. red fluorescence and green

Table 1. Experimental treatments. Total additions of deep water (as absolute values and % relative to the volume of the mesocosms), and nitrogen (N), phosphorus (P), and silica (Si). N, P, and Si values include both inorganic and organic forms, and represent the sum of all the net nutrient inputs of each water replacement.

Mesocosm	Upwelling mode	Upwelling intensity	Added deep water [m^3]	Added deep water [%]*	Added N [μmol L^{-1}]	Added P [μmol L^{-1}]	Added Si [μmol L^{-1}]
M5	Control		0.0	0.0	0.00	0.000	0.00
M3	Singular	Low	2.8	6.4	1.62	0.094	0.74
M7		Medium	5.3	12.0	3.07	0.177	1.41
M9		High	9.8	22.4	5.56	0.325	2.63
M1		Extreme	17.2	39.2	9.80	0.567	4.58
M2	Recurring	Low	2.8	6.3	1.61	0.094	0.69
M4		Medium	5.6	12.7	3.15	0.187	1.35
M6		High	11.2	25.6	6.16	0.363	2.64
M8		Extreme	22.4	51.1	10.97	0.682	4.96

*Considering average mesocosm volume of 43.775 m^3.

fluorescence vs. side scatter cytograms. Additionally, nano- and picophytoplankton abundances were determined by analyzing subsamples with no staining, and subgroups identified in red vs. orange fluorescence and red fluorescence vs. side scatter cytograms.

Viability of prokaryotic cells was quantified by flow cytometry through nucleic-acid double-staining using SYBR Green I and propidium iodide (Falcioni et al. 2008) following Baltar et al. (2010). Viable (intact cell membrane; live and potentially active) and non-viable (compromised cell membrane; dead or injured) cell populations were identified in green vs. red fluorescence cytograms.

Single-cell translational activity of prokaryotes

The single-cell translational (i.e., protein-synthesizing) activity of prokaryotes was assessed by BioOrthogonal Non-Canonical Amino acid Tagging (BONCAT) following Leizeaga et al. (2017). A detailed description of the entire procedure can be found in the Methods section of the Supporting Information for this article. Briefly, for each sampling time and mesocosm two replicates and a control (9 mL each) were incubated with L-Homopropargylglycine at a final concentration of 1 μmol L^{-1} for 2 h at in situ temperature. Incubations were fixed with paraformaldehyde at a final concentration of 2% (v/v) (controls were fixed before incubations). Samples were gently filtered through polycarbonate filters with a pore size of 0.2 μm (Whatman Nuclepore), and the filters were washed thrice with sterile ultrapure water, labeled, and stored at −80°C until further processing. To visualize translational activity, filters were subjected to Cu(I)-catalyzed click chemistry, labeling the newly synthesized proteins with Alexa594 azide dye (ThermoFisher). Lastly, filters were also counterstained with 4′,6-diamidino-2-phenylindole (DAPI; 1 μg mL^{-1} final concentration) to quantify total prokaryotic cells and were placed in microscope slides with antifading reagent (77% glycerol, 15% VECTASHIELD, and 8% 20× PBS).

Image acquisition to quantify translationally active cells was done in black and white with a Zeiss Axio Imager.Z2m Epifluorescence Microscope connected to a Zeiss camera (AxioCam MRm, Carl Zeiss MicroImaging, S.L., Barcelona, Spain) at 630× magnification, along with the AxioVision software. A Colibri LED light source (Carl Zeiss) with multiple light-emitting diodes was used, capturing all images at excitations of 385 nm (for DAPI) and 590 nm (for Alexa594), adjusting exposure time to optimize cell detection. Image analysis to quantify total (DAPI) and translationally active (BONCAT+) cells was carried out with the ACMEtool software.

Complementarily, bulk activity of prokaryotes (as prokaryotic heterotrophic production, PHP) was estimated from ^{3}H-leucine incorporation using the centrifugation method (Smith and Azam 1992), as detailed in the Methods section of the Supporting Information for this article.

DNA sampling, extraction, and sequencing

Using a peristaltic pump, samples were prefiltered through a 200 μm mesh to remove any large organisms and subsequently filtered through a set of polycarbonate filters with a pore size of 3.0 and 0.2 μm (Whatman Nuclepore), resulting in a size fractionation of 0.2–3.0 μm (hereafter "0.2 μm" size fraction) and 3.0–200 μm (hereafter "3.0 μm" size fraction). Upon filtration, filters were stored in autoclaved safe-lock tubes and kept at −80°C until further processing.

DNA extraction was performed using the DNeasy Plant Mini Kit (Qiagen) following instructions from the manufacturer. To increase extraction yield, the procedure was modified to include a pre-treatment of samples that consisted of (1) an initial (triple) freeze fracture step, (2) bead beating with autoclaved zirconia (0.1 mm) and glass (0.5 mm) beads (Sigma-Aldrich) for 5′, and (3) a proteinase-K (Sigma-Aldrich) treatment at 55°C for 1 h. Three polycarbonate filters with no sample were also subject to the extraction protocol to act as negative controls.

The extracted DNA was sequenced for the V4 and V5 regions of the 16S rRNA gene (16S rDNA) using the universal primers "515F" and "926R" (Parada et al. 2016). Amplified regions were sequenced with the Illumina MiSeq platform (paired-end reads; 2 × 250 bp) at the Argonne National Laboratory (Lemont, IL, USA).

16S amplicon sequence analysis

Bioinformatic analyses were performed at the Marine Bioinformatics platform (Marbits, marbits.icm.csic.es) of the Institut de Ciències del Mar (ICM-CSIC, Barcelona). *Cutadapt* (Martin 2011) was used to ensure primers were not present in the sequences. All subsequent analyses were performed in R (v. 4.0; R Core Team 2021). The *DADA2* package (Callahan et al. 2016) was used to process the amplicon sequence data (*trunclen* = (240, 155), *maxEE* = (2, 8), *minOverlap* = 15). Briefly, *DADA2* models errors in the Illumina-sequenced amplicon reads to infer exact amplicon sequence variants (ASVs) down to one nucleotide difference. Taxonomic assignation of ASVs was carried out using the "*assignTaxonomy*" function (*minBoot* = 50), with SILVA v. 138.1 (arb-silva.de) as the training set. Identification of contaminant sequences was performed using the *decontam* package (Davis et al. 2018) combining the frequency and prevalence methods (*threshold* = 0.2). Amplicon sequence variants classified as mitochondria and chloroplasts were also removed in this step. Average read retention was 57% (Supporting Information Fig. S1). Samples with at least 2500 reads were preserved for downstream analyses (247 out of 252). Preserved samples had an average sequencing depth of 13,920 reads (sd = 4567), encompassing a total of 9478 ASVs.

Statistical analyses

All statistical analyses were carried out in R (v. 4.1.2; R Core Team 2021). Non-metric multidimensional scaling (NMDS) was performed with the *metaMDS* function (*vegan* package, v. 2.5.7; Oksanen et al. 2020) to assess similarities in prokaryotic community composition among samples. A centered log ratio (CLR) transformed ASV count table with an added pseudocount of 1 was used for this analysis (*clr* function, *compositions* package, v. 2.0.4; van den Boogaart et al. 2022). Dissimilarities between day 3 (last preaddition sampling) and the rest of the samples within each size fraction were considered, and differences between treatments were evaluated by means of Kruskal-Wallis and post hoc Conover tests, correcting *p*-values with the Bonferroni method (*kruskalTest* and *kwAllPairsConoverTest* functions, *PMCMRplus* package, v. 1.9.6 [Pohlert 2022]). Correlations between changes in community composition and changes in environmental parameters were assessed through Mantel tests (*mantel* function, *vegan* [Legendre and Legendre 2012]) between sample dissimilarity matrices (Euclidean distances) based on (1) the CLR-transformed ASV abundance table and (2) the individual biogeochemical parameters. Diversity indicators of richness (number of ASVs) and evenness (Pielou index) were estimated with the *richness* and *evenness* functions (*microbiome* package, v. 1.16.0 [Lahti and Shetty 2019]), respectively, from a rarefied table of 5000 counts (sample $n = 241$) based on 100 permutations (*rrarefy.perm* function, *EcolUtils* package, v. 0.1; Salazar 2022).

Temporal patterns within prokaryotic communities were analyzed by Fuzzy C-Means Clustering (Bezdek 1981), which, for each element (here ASV), assigns a membership score for all clusters concurrently (from 0 to 1). Fuzzy clustering was performed individually for each treatment and size fraction combination using the *cmeans* function (*e1071* package, v. 1.7.9; Meyer et al. 2021). The fuzzifier parameter *m* was estimated following Schwämmle and Jensen (2010), resulting in a value (excluding deep waters) of 1.290 ± 0.025 (mean ± sd). The choice of the number of clusters (*k*) was based on several cluster selection indices (Within Cluster Sum of Squared Error, Simple Structure Index (*cascadeKM* function, *vegan*; Dimitriadou et al. 2002) and Normalized Partition Coefficient (*vegclustIndex* function, *vegan*; Bezdek 1981)) (Supporting Information Fig. S2), aiming to avoid redundant clusters (evaluated visually and through correlations). For this analysis, only ASVs representing at least 0.1% of reads in one sample were considered. To cluster ASVs according to their temporal patterns and exclude the influence of abundance levels, the CLR-transformed abundance of each ASV was centered and scaled by subtracting its mean and dividing by its standard deviation.

Ancillary environmental parameters

Descriptions of the procedures for the determination of ancillary environmental parameters reported in previous publications can be found in the Methods section of the Supporting Information for this article.

Results

Phytoplankton bloom dynamics

Simulated upwelling led to large diatom blooms, resulting in increases in primary production rates (Ortiz et al. 2022a). In the singular mode Chl *a* peaked on day 9 (11.2 $\mu g\ L^{-1}$ in the Extreme treatment, Fig. 1a), and blooms collapsed shortly afterward, while in the recurring treatments, the periodic deep water additions resulted in various blooms along the duration of the experiment, with oscillating Chl *a* concentrations and primary production rates (Ortiz et al. 2022a). Diatom community composition displayed some differences between upwelling modes: biomass estimates showed that singular treatments were dominated by *Leptocylindrus danicus* and *Guinardia striata*, while in the recurring treatments the taxa contributing most to biomass were *Leptocylindrus danicus* and *Leptocylindrus minimus*, except in the Extreme R, where *Dactyliosolen* sp. also presented high contributions (Ortiz et al. 2022b). Particulate organic carbon (POC) accumulated following the diatom blooms (Baumann et al. 2021) (Fig. 2a). Singular treatments presented the highest concentrations after the initial bloom (67 $\mu mol\ L^{-1}$), followed by a steady decrease. In the recurring treatments, increases were slower but POC accumulated until day ~ 19.

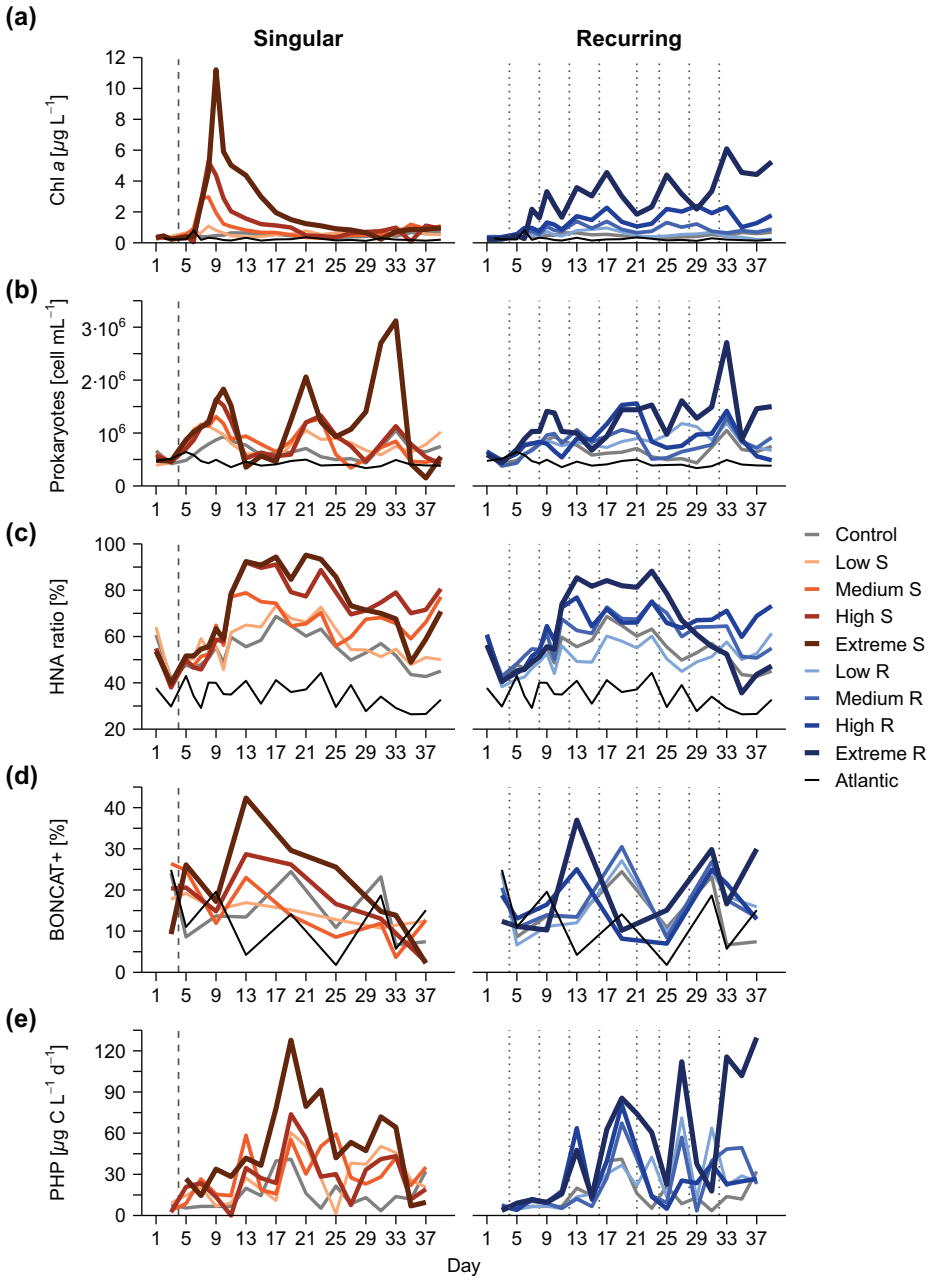

Fig. 1. Temporal dynamics of relevant biological variables. (**a**) Chlorophyll *a* (Chl *a*) concentration, (**b**) abundance of prokaryotes, (**c**) relative abundance of high nucleic acid content (HNA) prokaryotes, (**d**) relative abundance of prokaryotic cells actively synthesizing proteins (BONCAT+ cells), and (**e**) prokaryotic heterotrophic production (PHP). Results are displayed separately for singular (left column) and recurring treatments (right column). Vertical lines represent deep water additions (dashed = singular, dotted = recurring).

During the final days, the Extreme R treatment presented increases in POC (102 μmol L^{-1}), Chl *a* (5.2 μg L^{-1}), and primary production associated with a coccolithophorid bloom (Ortiz et al. 2022a). Dissolved organic carbon (DOC) accumulated proportionally to upwelling intensity during the decay of the initial blooms, followed by relatively stable concentrations across treatments ($\sim$ 140 μmol L^{-1} in Extreme treatments, Fig. 2b). Dissolved organic carbon accumulations happened in parallel to changes in the optical properties of dissolved organic matter (DOM), hinting prokaryotic DOM transformation and increased recalcitrance (*see* Gómez-Letona et al. 2022 for more details).

Prokaryotic abundance, viability, and activity

Prokaryotic abundance was between 3.8 and 4.9 $\times$ 10^5 cells mL^{-1} before the first deep water addition (Fig. 1b). After the additions, despite differences in magnitude, all mesocosms

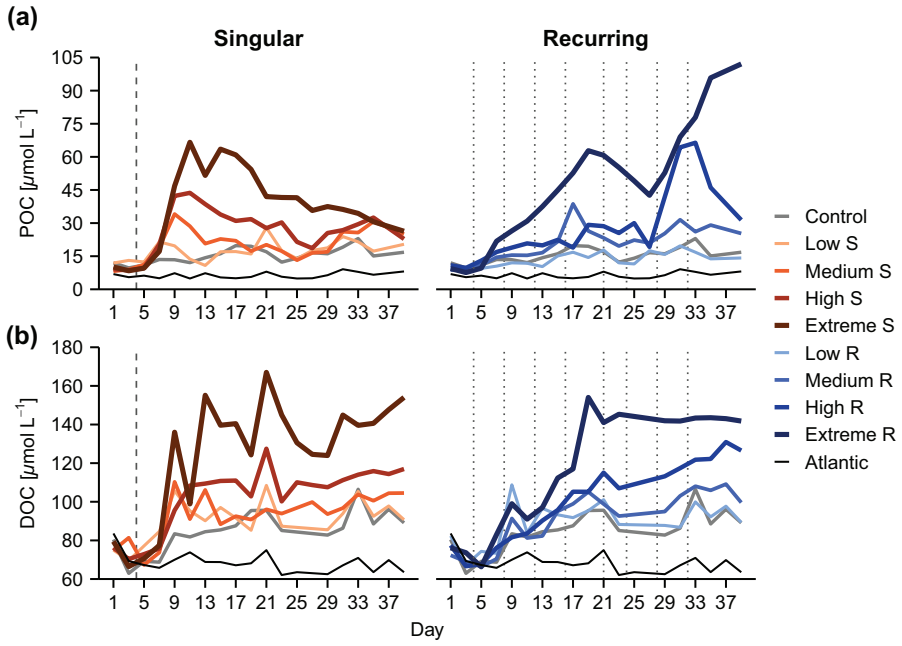

Fig. 2. Temporal dynamics of organic matter. (**a**) Particulate organic carbon (POC) and (**b**) dissolved organic carbon (DOC) during the experiment. Results are displayed separately for singular (left column) and recurring treatments (right column). Vertical lines represent deep water additions (dashed = singular, dotted = recurring). Data from Baumann et al. (2021) and Gómez-Letona et al. (2022), respectively.

followed similar trends, regardless of treatment: cell counts increased and first peaked on days 9–10 (up to 1.8×10^6 cells mL^{-1} in the Extreme S), slightly later than the initial diatom blooms (days 8–9). Abundances decreased on days 13–17, coinciding with the decay of the initial diatom blooms and an increase in the contribution of HNA prokaryotes (Fig. 1c). Abundances peaked again around day 21 and a last maximum was registered on day 33, reaching up to 3.1×10^6 and 2.7×10^6 cells mL^{-1} in the Extreme S and Extreme R treatments, respectively. The percentage of viable prokaryotes (i.e., those with intact cell membranes) was high throughout the experiment (> 85%, Supporting Information Fig. S3) but overall displayed three oscillations that tended to follow prokaryotic abundances (correlations between abundance and viability were significant in the Extreme treatments, Supporting Information Fig. S3).

The proportion of protein-synthesizing prokaryotes (BONCAT + cells, Fig. 1d) varied from (10–25) to 40% of total cells before the initial deep water addition to ~ 40% on day 13 in the Extreme treatments, evidencing an enhancement in the single-cell activity during the bloom decay. In fact, in stark contrast to the initial conditions and the Control mesocosm (Fig. 3a and Supporting Information Figs. S4 and S5), on day 13 clusters of highly active prokaryotes were observed attached to gel structures and particles (Fig. 3b and Supporting Information Fig. S4). After day 13 the upwelling modes showed two different outcomes: while the fraction of BONCAT+ cells decreased in the singular mode (falling below ~ 10% by day 37), the recurring mode registered values that oscillated between 10% and 30% BONCAT+ cells, with the Extreme and High treatments showing peaks on days 13 and 31 and the rest of the treatments showing a similar trend to the control mesocosm, with maxima on day 19. A notable peak in the proportion of BONCAT+ cells was observed at the end of the experiment in the Extreme R treatment, in parallel with the coccolithophorid bloom (Ortiz et al. 2022a). This activity peak coincided with the proliferation of active filamentous prokaryotes in this mesocosm (10–25 μm long, identified as Bacteroidetes through CARD-FISH, Supporting Information Fig. S6), in clear opposition to the low BONCAT signal observed in the Extreme S treatment (Fig. 3c,d).

Bulk activity levels, measured as PHP (Fig. 1e), showed different trends in the Extreme treatments of both modes. In the singular mode, PHP increased steadily until day 15, and increased sharply afterward, peaking on day 19 (128 μg C L^{-1} d^{-1}), coinciding with the rise of the second prokaryotic abundance peak, and showing a second peak around day 31. Conversely, in the Extreme R treatment, PHP showed marked oscillations that followed the peaks in Chl *a* (Fig. 1e). While in most mesocosms PHP decreased after day 33, the Extreme R treatment showed very high PHP rates during the final days, reaching 130 μg C L^{-1} d^{-1}. Low and medium intensity treatments showed similar trends regardless of mode. Despite the differences in the individual mesocosms, cumulative PHP was similar in both upwelling modes (Supporting Information Fig. S7).

General prokaryotic community composition

The composition of prokaryotic communities presented two main patterns: a temporal change, and a clear segregation between the two size fractions (Fig. 4a,b). Initial communities

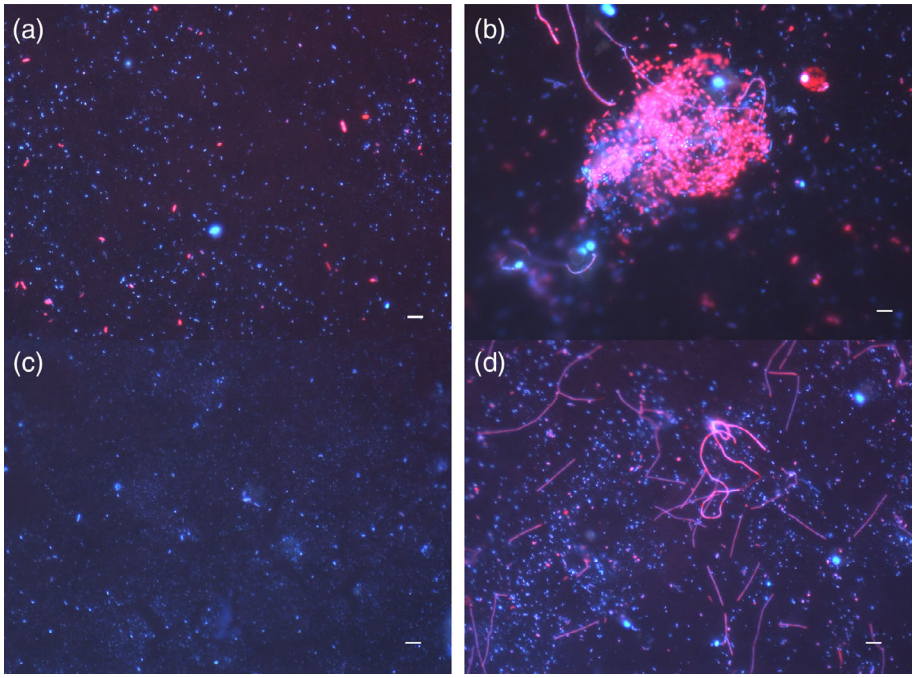

Fig. 3. Changes in single-cell protein synthesizing activity, spatial distribution, and morphology of prokaryotes. Images show the combined signal of 4′,6-diamidino-2-phenylindole (DAPI; all cells, blue) and Alexa594 (BONCAT+, protein-synthesizing cells, red) during key stages of the experiment in the Extreme treatments: (**a**) initial oligotrophic conditions (day 3, Extreme S), (**b**) diatom bloom decay (day 13, Extreme S), and (**c**) and (**d**) late senescence stage (Extreme S, day 37; and Extreme R, day 37, respectively). Scale bars (bottom right of each panel) represent 5 μm. Images for the Extreme R treatment on days 3 and 13 are available in Supporting Information Fig. S4 and for the Control on days 3, 13, and 37 in Supporting Information Fig. S5.

(day 3) within each size fraction were similar among treatments and ambient waters (Fig. 4a,b), the most abundant taxa being Flavobacteriales (23% of reads on average), Rhodobacterales (21%), the SAR11 clade (16%), Synechococcales (12%), and Actinomarinales (7%) in the 0.2 μm size fraction, and Flavobacteriales (37%), Rhodobacterales (16%), Pirellulales (9%), Synechococcales (5%), and Chitinophagales (5%) in the 3.0 μm size fraction (Supporting Information Fig. S8). The surface communities contrasted with the collected deep water, which was markedly dominated by members of Pseudomonadales and Rhodobacterales (Supporting Information Fig. S8). Euclidean distances between day 3 (last pre-addition sampling) and the rest of the samples showed that major changes occurred after upwelling induction (Fig. 4c). Changes in community composition tended to be larger in those treatments where the simulated upwelling was more intense, although differences were generally not significant ($p > 0.05$, Post-hoc Conover test, adjusted by Bonferroni method). Significant differences were also absent when comparing upwelling modes. Mantel tests showed significant correlations between changes in community composition in the 0.2 and 3.0 μm size fractions within each mesocosm (especially in the singular mode; Supporting Information Fig. S9).

Diversity estimates (Supporting Information Fig. S10) showed that, overall, richness (as number of ASVs present in a sample) decreased with time in the 0.2 μm size fraction, but taxa were evenly distributed over time (as defined by the Pielou index). On the contrary, in the 3.0 μm size fraction, there was a marked initial decrease in both richness and evenness after the first deep water addition, particularly in the singular treatments, but values returned close to initial ones shortly afterward (Supporting Information Fig. S10).

Temporal succession patterns

To facilitate the visualization of the dynamics of the prokaryotic communities in the different treatments, ASV temporal trends were grouped using fuzzy clusters (*see* Materials and methods section). These unveiled that prokaryotic successions occurred in four phases (i.e., clusters of ASVs) in all treatments, although there was an additional short-lived response in the singular treatments after the deep water additions (Fig. 5 and Supporting Information Fig. S11). The clusters identified were: (1) the initial community (named "*initial*"), (2) a group of ASVs dominating after the initial deep water addition, on days 5–7, only detected as a separate cluster in the singular treatments ("*postaddition*"), (3) a cluster peaking during the decay of the initial diatom blooms (days 11–19, "*postbloom*"), (4) a fourth one usually occurring during days 19–27 ("*intermediate*"), and (5) a final cluster dominating towards the end of the experiment ("*final*"). The temporal dynamics of the clusters were similar in the two size fractions (Fig. 5), overall displaying significant correlations (Supporting Information Fig. S12). While the

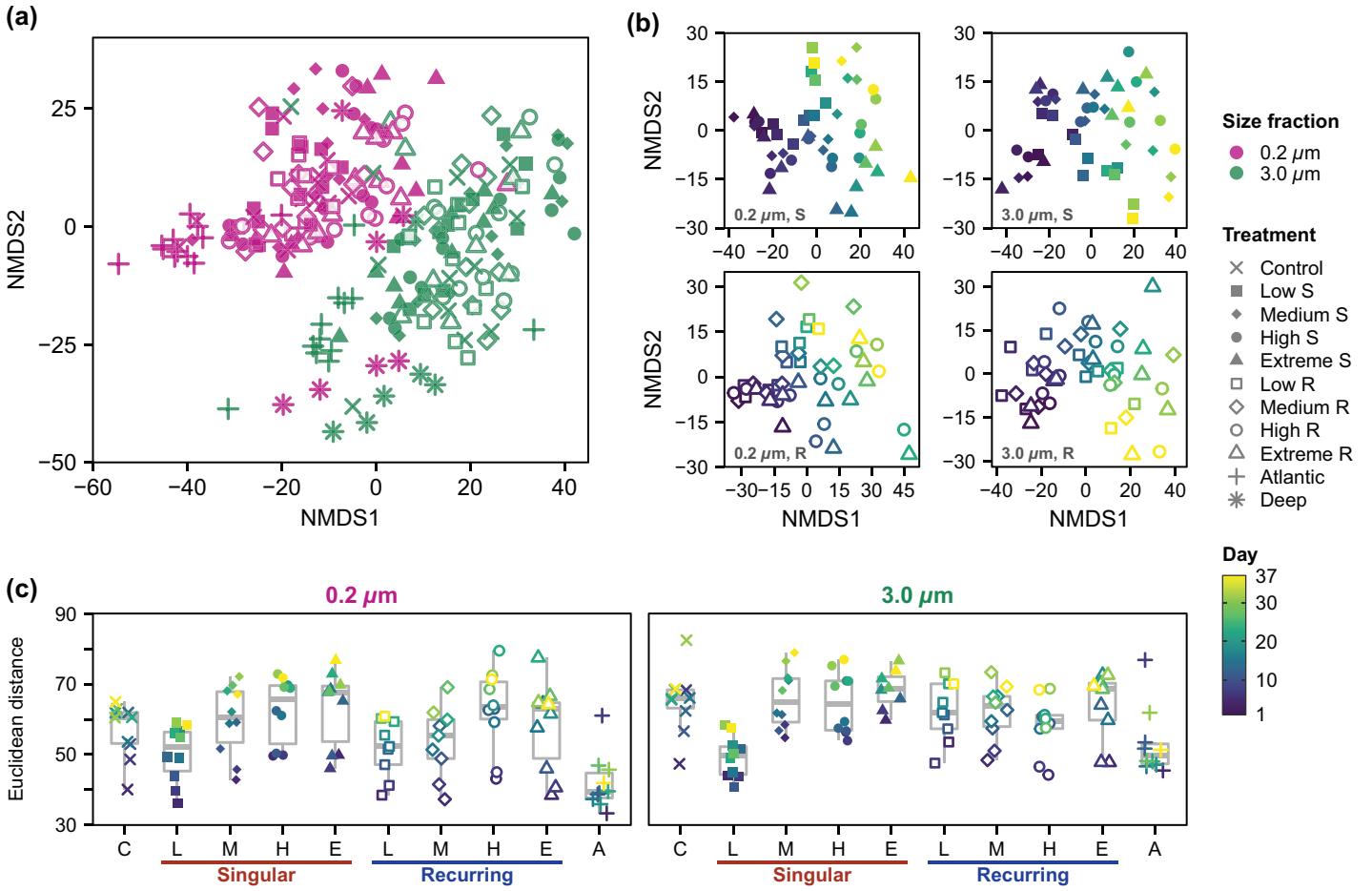

Fig. 4. Temporal changes in the prokaryotic community structure across upwelling scenarios. (**a**) Distribution of samples in the NMDS space according to their taxonomic composition, based on Euclidean distances estimated from the CLR-transformed ASV table. Each point corresponds to a sample, color representing the size fraction and shape of the experimental treatment. (**b**) Detailed NMDSs, computed separately for each upwelling mode (*S* and *R*) and size fraction (0.2 and 3.0 μm). The colormap represents the sampling day. (**c**) Euclidean distances between day 3 (last pre-addition sampling) and the rest of the samples (the colormap represents the sampling day), within each treatment and size fraction, estimated from the same CLR-transformed table. Labels on the X axis correspond to the initials of the treatments. Boxplots in the background summarize dissimilarities for each treatment: the horizontal line corresponds to the median; the lower and upper hinges correspond to the 25th and 75th percentiles; the upper (lower) whisker extends from the hinge to the largest (smallest) value no further than 1.5 * IQR from the hinge, where IQR is the inter-quartile range, that is, the distance between the 25th and 75th percentiles.

postaddition cluster was only resolved in the singular treatments (in agreement with the larger volume of deep water added, Table 1), ASVs that dominated this cluster (e.g., *Sulfitobacter*) appeared in the recurring treatments too after the first addition, but the response was not intense enough to conform an individual cluster (Fig. 6 and Supporting Information Fig. S13). The summed abundance of ASVs belonging to the individual clusters along the succession represented up to 54.9% ± 14.1% of the reads (mean ± sd of sum of ASV contributions during cluster peaks across treatments, Fig. 5 and Supporting Information Fig. S14).

Although similar successional trends were observed in all treatments, regardless of upwelling mode and size fraction, some differences were observed in terms of taxonomic composition, particularly between the singular and recurring modes (Fig. 6 and Supporting Information Fig. S13). The most representative ASVs of the initial clusters (which dominated the first few days of the experiment but decreased after simulated upwelling was initiated) belonged to multiple Flavobacteriales (notably, NS4, NS5, NS9, and NS2b marine groups), Rhodobacterales (chiefly HIMB11 genus), Actinomarinales, the SAR11 clade, and Synechococcales (Fig. 6 and Supporting Information Fig. S13). In some instances, the top two Synechococcales ASVs displayed no clear clustering and were present for most of the experiment (data not shown). In the singular treatments, which received the largest unique pulses of upwelling, the initial community was quickly overtaken by the postaddition cluster, formed by prokaryotes linked to deep waters. In this cluster, two Rhodobacterales ASVs from the *Sulfitobacter* genus (which dominated initial deep waters,

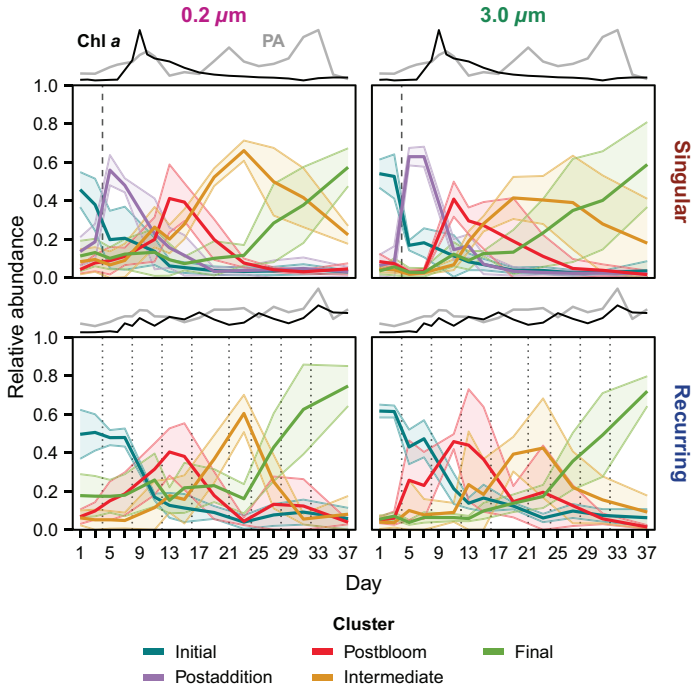

Fig. 5. Combined relative abundance of ASVs assigned to each cluster, averaged per upwelling mode (singular = upper row; recurring = lower row) and size fraction (0.2 μm = left column; 3.0 μm = right column). The shaded area around lines represents the ± standard deviation of averaged values across intensity treatments. Lines on top of plots show scaled Chl *a* (black) and prokaryotic abundance (PA, gray) values from Extreme treatments, in arbitrary units. Deep water additions are shown as dashed (singular) and dotted lines (recurring). Detailed results for all individual treatments are available in Supporting Information Fig. S14.

Supporting Information Fig. S13) were disproportionately abundant (32%–45% of reads) in both size fractions. Other Rhodobacterales (such as *Shimia* and *Planktotalea*) also contributed to the high relative abundance displayed by this order (Fig. 6 and Supporting Information Fig. S15). Likewise, some Pseudomonadales (e.g., *Pseudohongiella*) and Flavobacteriales (e.g., *Formosa*) were characteristic of the postaddition clusters (Fig. 6 and Supporting Information Fig. S13). In the recurring treatments, some of these ASVs also peaked on days 5–7, but due to their less prominent maxima they were clustered within the initial cluster (Fig. 6 and Supporting Information Fig. S13), increasing its temporal span, which was extended for longer than in the singular mode.

The postbloom cluster was associated with the decay of the initial diatom blooms and the DOC releases (Fig. 2b), and was mainly dominated by multiple Flavobacteriales (especially *Formosa* on days 7–13, followed on days 13–19 by other genera), some Rhodobacterales, Enterobacterales (such as *Vibrio* and *Alteromonas*), and Sphingobacteriales in the 0.2 μm size fraction of the Extreme treatments (Fig. 6a and Supporting Information Fig. S13). In the 3.0 μm size fraction, singular treatments prominently featured *Vibrio* (Enterobacterales) and *Cognatishimia* (Rhodobacterales), whereas the recurring treatments had a large representation of *Cognatishimia* and multiple other ASVs from diverse orders (Fig. 6b and Supporting Information Fig. S13).

The intermediate cluster peaked on days 19–27 across treatments (Fig. 5), coinciding with the stabilization of DOC concentrations (Fig. 2b). In the singular treatments the 0.2 μm size fraction was dominated by members of the OM60 (NOR5) clade (among other Pseudomonadales), Flavobacteriales, Rhodobacterales, and Puniceispirillales (Fig. 6 and Supporting Information Fig. S13). In the same size fraction of the recurring treatments, *Cognatishimia* dominated the intermediate cluster, together with several Flavobacteriales ASVs. The 3.0 μm size fraction of the singular treatments initially included *Lentilitoribacter* (among other Rhizobiales), but ended up dominated by *Croceitalea* (Flavobacteriales) (Fig. 6 and Supporting Information Fig. S13). In the recurring treatments, Rhodobacterales (again, predominantly *Cognatishimia*) were the most relevant taxa.

During the final days of the experiment, markedly different outcomes were observed for Extreme treatments, especially within the 3.0 μm size fraction. *Croceitalea* was the most prominent taxa in the singular upwelling, while in the recurring upwelling the community was dominated by Chitinophagales ASVs from the *Lewinella* and *Phaeodactylibacter* genera (they represented more than 50% of the community by day 37, Fig. 6b and Supporting Information Fig. S15).

Relationship between prokaryotic community composition and DOM

Taxonomic successions were strongly related to changes in the organic matter pools in each of the treatments (Supporting Information Fig. S16). The highest correlations between changes in community composition and environmental parameters were found with chromophoric DOM: particularly with a_{254} and a_{325}, proxies for its concentration, and $S_{275–295}$ and S_R, which indicate changes in its average molecular weight (*see* Gómez-Letona et al. 2022 for details). Likewise, taxonomic changes were highly associated with humic-like fluorescent DOM and, to a lesser extent, DOC concentrations and protein-like fluorescent DOM. The changes in these optical properties of DOM (both the chromophoric and fluorescent fractions) during the experiment were deemed to be signs of prokaryotic transformation of the DOM pool and of its increased recalcitrance (Gómez-Letona et al. 2022). Significant correlations were found with POM concentrations, which tended to be stronger for the recurring treatments. Changes in Chl *a* concentrations, biogenic silica, and added nutrient concentrations displayed higher correlations with taxonomic changes in the recurring treatments for both size fractions, but were overall low. Changes in diatom composition seemed to have a very weak role in structuring the prokaryotic communities (Supporting Information Fig. S16).

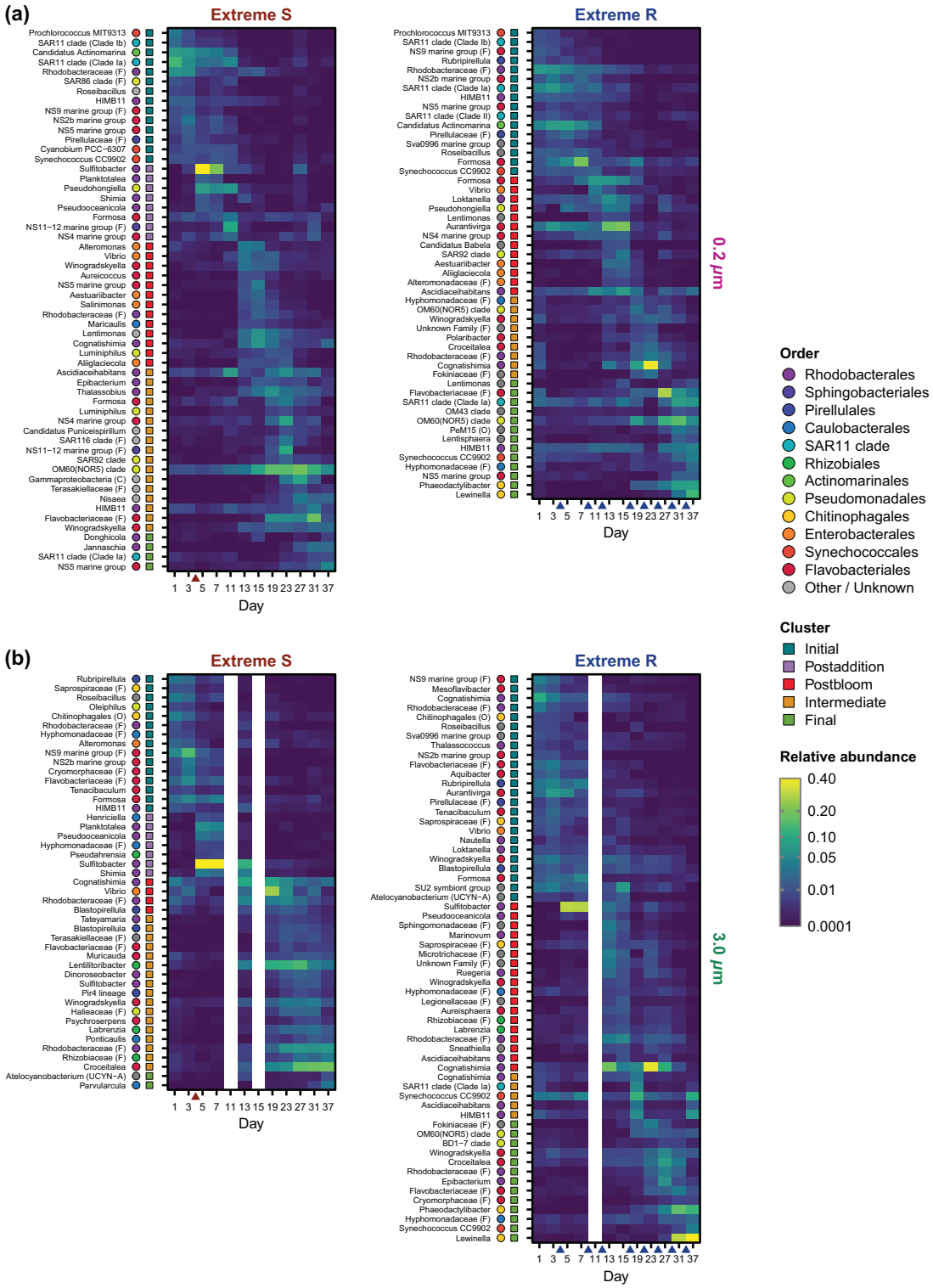

Fig. 6. Succession patterns of most relevant prokaryotic taxa. Results are shown for the Extreme S and Extreme R treatments in the (**a**) 0.2 μm and (**b**) 3.0 μm size fractions. For each cluster, treatment, and size fraction, ASVs with a membership value over 0.75 were merged by genera (when possible; otherwise, at the most detailed taxonomic level available, as indicated next to their name: F = family, O = order, C = class). From those, taxa representing at least 0.5% of reads in more than 1 sample within each treatment and size fraction are shown. Colormap represents relative abundance of taxa (note that to aid visualization (1) the scale is cubic-root-transformed and (2) out of bounds outlier values have been assigned the colors of the upper and lower limits of the colormap). Colored dots represent the taxonomic order of taxa, and colored squares their cluster assignation. Results for all the treatments are shown in Supporting Information Fig. S13.

Discussion

Influence of upwelling regimes on prokaryotic abundance and activity

Phytoplankton blooms are known to heavily influence the standing stocks and activity of prokaryotic communities, providing copious amounts of organic substrates among which polysaccharides such as laminarin occupy a prominent place (Becker et al. 2020; Reintjes et al. 2020). Increases in the average molecular weight of DOM during bloom decay (as indicated by proxies) (Gómez-Letona et al. 2022) and the presence of transparent exopolymer particles (Baumann et al. 2021) likely reflect such polysaccharide releases during the diatom blooms observed in this study. In contrast to the usual pattern where prokaryotic abundances peak during bloom termination and remain temporarily elevated (Buchan et al. 2014), we observed that standing stocks of prokaryotes quickly decreased across all treatments after reaching their peak. Given that conditions during bloom collapse were favorable for prokaryotic growth due to major DOM releases (Gómez-Letona et al. 2022), the decrease in prokaryotic abundance was probably related to a rapid top-down control through grazing by flagellates and/or viral infection (Riemann et al. 2000). The considerable viability drops around day 13 likely reflect these top-down mortality losses (Supporting Information Fig. S3). The two subsequent peaks in cell counts occurred in both modes, even if diatom blooms and new production were sustained only in the recurring treatments (Ortiz et al. 2022b). Substrates fueling such continued proliferation cycles of prokaryotes in the singular mode, where diatom blooms collapsed, likely arose from organic matter recycling within the prokaryotic community itself. Storage alpha-glucans potentially played an important role, particularly following the mortality episodes of each abundance cycle (Sidhu et al. 2023; Beidler et al. 2024). The less pronounced abundance drops in the recurring mode might indicate that prokaryotes engaged in significant recycling while continuing to benefit from new inputs of DOM from the sustained diatom blooms. Such influence of intra-community recycling across bloom scenarios could have contributed to the similar temporal dynamics in all upwelling modes.

Despite the decrease in cell counts after the first bloom peak (~ day 13), the proportion of prokaryotes that were actively synthesizing proteins overall peaked around this time, evidencing that a considerable fraction of the remaining prokaryotes was active (Fig. 1d). Microscopy images indicated that many of these prokaryotes were attached to the surface of particles and gel structures (Fig. 3 and Supporting Information Fig. S4), consuming and transforming the organic matter released by decaying phytoplankton (Engel et al. 2002). The marked differences in activity patterns between the Extreme S and Extreme R treatments at the end of the experiment (Figs. 1d,e and 3), while cumulative PHP being similar (Supporting Information Fig. S7), suggest that the upwelling mode could impact the timing of carbon cycling by microbial communities. Moreover, the marked activity differences between prokaryotes within specific communities (Fig. 3 and Supporting Information Fig. S4) evidence how different groups could have contrasting contributions to organic matter cycling (Munson-McGee et al. 2022).

The observed percentage of active cells was lower than expected when compared with previous BONCAT observations in oligotrophic waters (Leizeaga et al. 2017), although it was in line with MAR-FISH-based activity reports from the Canary Current upwelling system (Alonso-Sáez et al. 2012). Difficulties discriminating closely clustered cells (e.g., Fig. 3b), insufficient substrate concentration at very high cell densities (up to 3×10^6 cells mL^{-1}) and competition by highly active eukaryotic phytoplankton (Supporting Information Fig. S17), known to incorporate amino acids through osmotrophy (Mena et al. 2024), are factors that could have reduced the sensitivity of our measurements and, thus, these results should be considered as an indicator of activity changes within the prokaryotic communities rather than a precise estimate of the fraction of active cells.

Prokaryotic successions show consistent temporal patterns

Prokaryotic community successions during phytoplankton blooms are thought to be tightly coupled with the different algal bloom stages (Zhou et al. 2019). Yet, we observed surprisingly similar succession dynamics across size fractions and upwelling scenarios (Fig. 5), despite the differences in bloom outcomes regarding the timing of the bloom peak, its intensity and duration (Fig. 1a and Ortiz et al. 2022a). Although there were some differences in the specific taxa populating the successional stages in the different mesocosms, some general trends emerged. Initial communities, adapted to low nutrient conditions (e.g., the SAR11 clade, Giovannoni 2017), were displaced during the first few days. While, in the singular mode, these were superseded consecutively by postaddition and postbloom prokaryotes, in the recurring treatments communities proceeded directly to the postbloom stage. This difference arose as a result of the lower volumes of deep water that were introduced in the recurring mode, resulting in a low prevalence of taxa linked to the postaddition cluster. The postbloom communities, associated with the decay of the initial phytoplankton bloom, were composed of copiotrophic specialists such as Flavobacteriales and Enterobacterales (*Alteromonas*, *Vibrio*), known to be highly efficient consuming phytoplankton-derived organic matter (including alpha- and beta-glucans; Koch et al. 2019; Krüger et al. 2019; Sidhu et al. 2023). Moreover, *Alteromonas* are specially active colonizing particles (Ivars-Martínez et al. 2008; Boeuf et al. 2019), a trait that is coherent with their enhanced abundances during this phase in parallel with a large increase in particulate organic matter (Baumann et al. 2021). Some members of Rhodobacterales were also characteristic of the postbloom phase, despite they do not always appear to respond to DOM inputs during phytoplankton bloom decay (Pontiller et al. 2022). The following phase of the successions featured Flavobacteriales and Rhodobacterales, which may have

participated in the recycling of bacterial biomass (Sidhu et al. 2023; Beidler et al. 2024) during the second abundance cycle. Other taxa potentially capable of degrading polysaccharides as well as aromatic compounds, such as the OM60 clade (Jang et al. 2011; Sidhu et al. 2023), were also prominent.

During the final days, there was a clear divergence between upwelling modes in terms of the dominant taxa. In the Extreme S treatment (and, to a lesser extent, in the other singular mesocosms) *Croceitalea* became the dominant taxon. Members of this genus have been shown to possess genes that encode for enzymes that participate in the degradation of polysaccharides and proteins (Kwon et al. 2016), which likely proved beneficial during the senescence phase of the phytoplankton bloom. These observations were in marked contrast to those of the Extreme R treatment, where two Saprospiraceae genera (*Lewinella* and *Phaeodactylibacter*) proliferated. By timing and morphology (Khan et al. 2007; Chen et al. 2014), these Saprospiraceae genera matched the highly active filamentous Bacteroidetes observed by fluorescence microscopy (Fig. 3d and Supporting Information Fig. S6), suggesting that their high abundances in the 3.0 μm size fraction were due to their filamentous nature, rather than a particle-attached lifestyle. At least some members of Saprospiraceae possess alpha-glucan polysaccharide utilization loci (Beidler et al. 2024) and have been observed to display high peptidase transcription during the senescence phase of diatom blooms (Pontiller et al. 2022). Expression of transcripts related to degradation of aromatic molecules has also been reported for *Phaeodactylibacter* (Lee et al. 2018). These metabolic traits might offer them an advantage over other taxa, although the specific reasons behind their proliferation coupled to the coccolithophorid bloom are unknown.

Composition shifts of particle colonizers (3.0 μm size fraction) paralleled those observed in the free-living community (0.2 μm size fraction) (Fig. 5 and Supporting Information Fig. S9), hinting that the temporal dynamics of both size fractions were related. Despite the taxonomic composition of both size fractions was different (Fig. 4a and Supporting Information Fig. S8), ASVs with particle-attached and dual lifestyles (with no significant differences between the 0.2 and 3.0 μm size fractions) presented considerably high relative abundances in the free-living community, notably during bloom decay in some mesocosms (Supporting Information Fig. S18). Such observation implies a potential connectivity between the two size fractions, involving colonization and detachment from particles (Kiørboe et al. 2003; Datta et al. 2016), which could have contributed to the parallelism in successions.

The correlations found between changes in community composition and changes in the DOM quantities and characteristics (Supporting Information Fig. S16), consistent in both upwelling modes despite the remarkably different bloom developments, suggest the functional successions we observed were related to the transformation of the organic matter pool. Paired with the repeating prokaryotic abundance cycles and the major presence of taxa capable of utilizing diverse polysaccharides (*see* previous discussion in this section), our observations seem to be in agreement with recent reports underlining the importance of intra-community recycling of prokaryotic biomass during phytoplankton blooms (Beidler et al. 2024). Thus, despite certain variability in the specific taxa, prokaryotic community dynamics and successional patterns seemed to be more coupled with organic matter accumulation and transformation (which tended to be similar in both upwelling modes, Gómez-Letona et al. 2022), than with the concurrent bloom state (with markedly contrasting dynamics between upwelling modes, including some differences in diatom composition). This suggests that once prokaryotes reacted to the initial DOM release from the blooms, they seemed to be more influenced by intra-community processes rather than by continued new DOM inputs by phytoplankton. Trophic interactions (Gralka et al. 2020), viral lysis (Bartlau et al. 2022; Szabo et al. 2022), and/or predation (Allers et al. 2007) likely contributed to the observed dynamics by impacting prokaryotes and the recycling of their biomass. Modeling approaches such as the study of model organisms (Koch et al. 2019), synthetic communities and environments (Bunse et al. 2021; Deng et al. 2022), and numerical simulations (Kerimoglu et al. 2022) could help to disentangle the influence of all these different factors and improve our understanding of the microbial interactions and the utilization of organic substrates during succession processes of free-living and particle-attached prokaryotes.

Studying prokaryotic community dynamics under phytoplankton blooms of varying characteristics advances our understanding on how these ecological processes develop and how they contribute to the marine carbon cycle. By simulating contrasting upwelling scenarios using large-scale mesocosms, we triggered distinct phytoplankton bloom events and showed that, despite differences in activity, prokaryotic successions tended to share temporal patterns across upwelling scenarios and size fractions, regardless of phytoplankton bloom intensity and duration. Our results suggest that prokaryotic successions seem to be more associated with processes of organic matter accumulation, transformation, and recycling within the community, rather than being tightly coupled with the development of phytoplankton blooms. This contrasted with the prokaryotic heterotrophic activity, which, although cumulatively similar, differed in timing in the two upwelling modes, suggesting that the precise way in which organic matter is cycled by prokaryotes might be influenced by bloom patterns. These findings enhance our comprehension of how microbial ecological successions and carbon cycling unfold under varying phytoplankton bloom scenarios.

Data availability statement

Flow cytometry (abundances, viability) and BONCAT results are available in the PANGAEA repository (www.pangaea.de) under accession number 964544 (Gómez-Letona et al. 2024). All other ancillary biogeochemical parameters are

also available in PANGAEA and/or can be found in their respective publications: Baumann et al. (2021) for inorganic nutrients, PHP, and particulate organic matter; Ortiz et al. (2022b) for Chl *a* measurements and diatom community composition; Ortiz et al. (2022a) for fractionated Chl *a*; and Gómez-Letona et al. (2022) for all dissolved organic matter variables. The sequencing data for this study have been deposited in the European Nucleotide Archive at EMBL-EBI (www.ebi.ac.uk/ena) under accession number PRJEB67976.

References

Allers, E., L. Gómez-Consarnau, J. Pinhassi, J. M. Gasol, K. Šimek, and J. Pernthaler. 2007. Response of Alteromonadaceae and Rhodobacteriaceae to glucose and phosphorus manipulation in marine mesocosms. Environ. Microbiol. **9**: 2417–2429. doi:10.1111/j.1462-2920.2007.01360.x

Alonso-Sáez, L., O. Sánchez, and J. M. Gasol. 2012. Bacterial uptake of low molecular weight organics in the subtropical Atlantic: Are major phylogenetic groups functionally different? Limnol. Oceanogr. **57**: 798–808. doi:10.4319/lo.2012.57.3.0798

Azam, F., and F. Malfatti. 2007. Microbial structuring of marine ecosystems. Nat. Rev. Microbiol. **5**: 782–791. doi:10.1038/nrmicro1747

Balmonte, J. P., M. Simon, H.-A. Giebel, and C. Arnosti. 2021. A sea change in microbial enzymes: Heterogeneous latitudinal and depth-related gradients in bulk water and particle-associated enzymatic activities from 30° S to 59° N in the Pacific Ocean. Limnol. Oceanogr. **66**: 3489–3507. doi:10.1002/lno.11894

Baltar, F., J. Arístegui, J. M. Gasol, I. Lekunberri, and G. J. Herndl. 2010. Mesoscale eddies: Hotspots of prokaryotic activity and differential community structure in the ocean. ISME J. **4**: 975–988. doi:10.1038/ismej.2010.33

Bartlau, N., A. Wichels, G. Krohne, E. M. Adriaenssens, A. Heins, B. M. Fuchs, R. Amann, and C. Moraru. 2022. Highly diverse flavobacterial phages isolated from North Sea spring blooms. ISME J. **16**: 555–568. doi:10.1038/s41396-021-01097-4

Baumann, M., and others. 2021. Effect of intensity and mode of artificial upwelling on particle flux and carbon export. Front. Mar. Sci. **8**: 742142. doi:10.3389/fmars.2021.742142

Becker, S., J. Tebben, S. Coffinet, K. Wiltshire, M. H. Iversen, T. Harder, K.-U. Hinrichs, and J.-H. Hehemann. 2020. Laminarin is a major molecule in the marine carbon cycle. Proc. Natl. Acad. Sci. **117**: 6599–6607. doi:10.1073/pnas.1917001117

Beidler, I., and others. 2024. Alpha-glucans from bacterial necromass indicate an intra-population loop within the marine carbon cycle. Nat. Commun. **15**: 4048. doi:10.1038/s41467-024-48,301-5

Bezdek, J. C. 1981. Pattern recognition with fuzzy objective function algorithms, 1st ed. Plenum Press. doi:10.1007/978-1-4757-0450-1

Bode, A., M. Álvarez, M. Ruíz-Villarreal, and M. M. Varela. 2019. Changes in phytoplankton production and upwelling intensity off A Coruña (NW Spain) for the last 28 years. Ocean Dyn. **69**: 861–873. doi:10.1007/s10236-019-01278-y

Boeuf, D., and others. 2019. Biological composition and microbial dynamics of sinking particulate organic matter at abyssal depths in the oligotrophic open ocean. Proc. Natl. Acad. Sci. **116**: 832. doi:10.1073/pnas.1903080116

Bograd, S. J., and others. 2023. Climate change impacts on eastern boundary upwelling systems. Ann. Rev. Mar. Sci. **15**: 303–328. doi:10.1146/annurev-marine-032122-021945

van den Boogaart, K. G., R. Tolosana-Delgado, and M. Bren. 2022. Compositions: Compositional data analysis. R package version 2.0-4 [accessed 2022 January 05]. Available from https://CRAN.R-project.org/package=compositions

Buchan, A., G. R. LeCleir, C. A. Gulvik, and J. M. González. 2014. Master recyclers: Features and functions of bacteria associated with phytoplankton blooms. Nat. Rev. Microbiol. **12**: 686–698. doi:10.1038/nrmicro3326

Bunse, C., H. Koch, S. Breider, M. Simon, and M. Wietz. 2021. Sweet spheres: Succession and CAZyme expression of marine bacterial communities colonizing a mix of alginate and pectin particles. Environ. Microbiol. **23**: 3130–3148. doi:10.1111/1462-2920.15536

Callahan, B. J., P. J. McMurdie, M. J. Rosen, A. W. Han, A. J. A. Johnson, and S. P. Holmes. 2016. DADA2: High-resolution sample inference from Illumina amplicon data. Nat. Methods **13**: 581–583. doi:10.1038/nmeth.3869

Capone, D. G., and D. A. Hutchins. 2013. Microbial biogeochemistry of coastal upwelling regimes in a changing ocean. Nat. Geosci. **6**: 711–717. doi:10.1038/ngeo1916

Chavez, F. P., and M. Messié. 2009. A comparison of eastern boundary upwelling ecosystems. Prog. Oceanogr. **83**: 80–96. doi:10.1016/j.pocean.2009.07.032

Chen, Z., and others. 2014. Phaeodactylibacter xiamenensis gen. Nov., sp. nov., a member of the family Saprospiraceae isolated from the marine alga Phaeodactylum tricornutum. Int. J. Syst. Evol. Microbiol. **64**: 3496–3502. doi:10.1099/ijs.0.063909-0

Cropper, T. E., E. Hanna, and G. R. Bigg. 2014. Spatial and temporal seasonal trends in coastal upwelling off Northwest Africa, 1981–2012. Deep-Sea res. Part I Oceanogr. Res. Pap. **86**: 94–111. doi:10.1016/j.dsr.2014.01.007

Datta, M. S., E. Sliwerska, J. Gore, M. F. Polz, and O. X. Cordero. 2016. Microbial interactions lead to rapid micro-scale successions on model marine particles. Nat. Commun. **7**: 11965. doi:10.1038/ncomms11965

Davis, N. M., D. M. Proctor, S. P. Holmes, D. A. Relman, and B. J. Callahan. 2018. Simple statistical identification and removal of contaminant sequences in marker-gene and

metagenomics data. Microbiome **6**: 226. doi:10.1186/s40168-018-0605-2

Deng, Y., M. Mauri, M. Vallet, M. Staudinger, R. J. Allen, and G. Pohnert. 2022. Dynamic diatom-bacteria consortia in synthetic plankton communities. Appl. Environ. Microbiol. **88**: e01619-22. doi:10.1128/aem.01619-22

Desbiolles, F., B. Blanke, and A. Bentamy. 2014. Short-term upwelling events at the western African coast related to synoptic atmospheric structures as derived from satellite observations. J. Geophys. Res. Ocean. **119**: 461–483. doi:10.1002/2013JC009278

Dimitriadou, E., S. Dolničar, and A. Weingessel. 2002. An examination of indexes for determining the number of clusters in binary data sets. Psychometrika **67**: 137–159. doi:10.1007/BF02294713

Engel, A., S. Goldthwait, U. Passow, and A. Alldredge. 2002. Temporal decoupling of carbon and nitrogen dynamics in a mesocosm diatom bloom. Limnol. Oceanogr. **47**: 753–761. doi:10.4319/lo.2002.47.3.0753

Falcioni, T., S. Papa, and J. M. Gasol. 2008. Evaluating the flow-cytometric nucleic acid double-staining protocol in realistic situations of planktonic bacterial death. Appl. Environ. Microbiol. **74**: 1767–1779. doi:10.1128/AEM.01668-07

Giovannoni, S. J. 2017. SAR11 bacteria: The most abundant plankton in the oceans. Ann. Rev. Mar. Sci. **9**: 231–255. doi:10.1146/annurev-marine-010814-015934

Gómez-Letona, M., M. Sebastián, I. Baños, M. F. Montero, C. P. Barrancos, M. Baumann, U. Riebesell, and J. Arístegui. 2022. The importance of the dissolved organic matter pool for the carbon sequestration potential of artificial upwelling. Front. Mar. Sci. **9**: 969714. doi:10.3389/fmars.2022.969714

Gómez-Letona, M., M. Sebastian, M. F. Montero, U. Riebesell, and J. Arístegui. 2024. KOSMOS 2018 gran Canaria mesocosm study: Prokaryotes. PANGAEA. doi:10.1594/PANGAEA.964544

Gralka, M., R. Szabo, R. Stocker, and O. X. Cordero. 2020. Trophic interactions and the drivers of microbial community assembly. Curr. Biol. **30**: R1176–R1188. doi:10.1016/j.cub.2020.08.007

Ivars-Martínez, E., A. B. Martín-Cuadrado, G. D'Auria, A. Mira, S. Ferriera, J. Johnson, R. Friedman, and F. Rodríguez-Valera. 2008. Comparative genomics of two ecotypes of the marine planktonic copiotroph Alteromonas macleodii suggests alternative lifestyles associated with different kinds of particulate organic matter. ISME J. **2**: 1194–1212. doi:10.1038/ismej.2008.74

Jang, Y., H.-M. Oh, I. Kang, K. Lee, S.-J. Yang, and J.-C. Cho. 2011. Genome sequence of strain IMCC3088, a proteorhodopsin-containing marine bacterium belonging to the OM60/NOR5 clade. J. Bacteriol. **193**: 3415–3416. doi:10.1128/JB.05111-11

Kerimoglu, O., and others. 2022. Growth, organic matter release, aggregation and recycling during a diatom bloom: A model-based analysis of a mesocosm experiment. bioRxiv: 2022.05.18.492269. doi:10.1101/2022.05.18.492269

Khan, S. T., Y. Fukunaga, Y. Nakagawa, and S. Harayama. 2007. Emended descriptions of the genus *Lewinella* and of *Lewinella cohaerens*, *Lewinella nigricans* and *Lewinella persica*, and description of *Lewinella lutea* sp. nov. and *Lewinella marina* sp. nov. Int. J. Syst. Evol. Microbiol. **57**: 2946–2951. doi:10.1099/ijs.0.65308-0

Kiørboe, T., K. Tang, H.-P. Grossart, and H. Ploug. 2003. Dynamics of microbial communities on marine snow aggregates: Colonization, growth, detachment, and grazing mortality of attached bacteria. Appl. Environ. Microbiol. **69**: 3036–3047. doi:10.1128/AEM.69.6.3036-3047.2003

Koch, H., and others. 2019. Biphasic cellular adaptations and ecological implications of *Alteromonas macleodii* degrading a mixture of algal polysaccharides. ISME J. **13**: 92–103. doi:10.1038/s41396-018-0252-4

Krüger, K., M. Chafee, T. Ben Francis, T. Glavina del Rio, D. Becher, T. Schweder, R. I. Amann, and H. Teeling. 2019. In marine Bacteroidetes the bulk of glycan degradation during algae blooms is mediated by few clades using a restricted set of genes. ISME J. **13**: 2800–2816. doi:10.1038/s41396-019-0476-y

Kuhlisch, C., G. Schleyer, N. Shahaf, F. Vincent, D. Schatz, and A. Vardi. 2022. Viral infection of algal blooms leaves a unique metabolic footprint on the dissolved organic matter in the ocean. Sci. Adv. **7**: eabf4680. doi:10.1126/sciadv.abf4680

Kwon, S.-K., H. G. Lee, M.-J. Kwak, and J. F. Kim. 2016. Genome sequence of the marine flavobacterium *Croceitalea dokdonensis* DOKDO 023 that contains proton- and sodium-pumping rhodopsins. Mar. Genomics **26**: 1–3. doi:10.1016/j.margen.2015.11.011

Lahti, L., and S. Shetty. 2019. Microbiome R package, version 1.16.0 [accessed 2021 October 26]. Available from http://microbiome.github.io

Leblanc, K., V. Cornet, M. Caffin, M. Rodier, A. Desnues, H. Berthelot, K. Turk-Kubo, and J. Heliou. 2016. Phytoplankton community structure in the VAHINE mesocosm experiment. Biogeosciences **13**: 5205–5219. doi:10.5194/bg-13-5205-2016

Lee, M. D., E. A. Webb, N. G. Walworth, F.-X. Fu, N. A. Held, M. A. Saito, and D. A. Hutchins. 2018. Transcriptional activities of the microbial consortium living with the marine nitrogen-fixing cyanobacterium *Trichodesmium* reveal potential roles in community-level nitrogen cycling. Appl. Environ. Microbiol. **84**: e02026–17. doi:10.1128/AEM.02026-17

Legendre, P., and L. Legendre. 2012. Numerical ecology. Elsevier.

Leizeaga, A., M. Estrany, I. Forn, and M. Sebastián. 2017. Using click-chemistry for visualizing in situ changes of translational activity in planktonic marine bacteria. Front. Microbiol. **8**: 2360. doi:10.3389/fmicb.2017.02360

Llinás, O., A. R. de León, G. Siedler, and G. Wefer. 1997. ESTOC Data Report 1994. 77.

Martin, M. 2011. Cutadapt removes adapter sequences from high-throughput sequencing reads. EMBnet.journal. **17**: 10–12. doi:10.14806/ej.17.1.200

Mena, C., and others. 2024. High amino acid osmotrophic incorporation by marine eukaryotic phytoplankton revealed by click chemistry. ISME Commun. **4**: ycae004. doi:10.1093/ismeco/ycae004

Meyer, D., E. Dimitriadou, K. Hornik, A. Weingessel, and F. Leisch. 2021. e1071: Misc functions of the Department of Statistics, probability theory group (formerly: E1071), TU Wien. R package version 1.7-9 [accessed 2021 September 16]. Available from https://CRAN.R-project.org/package=e1071

Moran, M. A. 2015. The global ocean microbiome. Science **350**: aac8455. doi:10.1126/science.aac8455

Mühlenbruch, M., H.-P. Grossart, F. Eigemann, and M. Voss. 2018. Mini-review: Phytoplankton-derived polysaccharides in the marine environment and their interactions with heterotrophic bacteria. Environ. Microbiol. **20**: 2671–2685. doi:10.1111/1462-2920.14302

Munson-McGee, J. H., and others. 2022. Decoupling of respiration rates and abundance in marine prokaryoplankton. Nature **612**: 764–770. doi:10.1038/s41586-022-05505-3

Needham, D. M., and J. A. Fuhrman. 2016. Pronounced daily succession of phytoplankton, archaea and bacteria following a spring bloom. Nat. Microbiol. **1**: 16005. doi:10.1038/nmicrobiol.2016.5

Oksanen, J., and others. 2020. Vegan: Community ecology package. R package version 2.5-7 [accessed 2020 November 28]. Available from https://CRAN.R-project.org/package=vegan

Ortiz, J., J. Arístegui, N. Hernández-Hernández, M. Fernández-Méndez, and U. Riebesell. 2022*a*. Oligotrophic phytoplankton community effectively adjusts to artificial upwelling regardless of intensity, but differently among upwelling modes. Front. Mar. Sci. **9**: 880550. doi:10.3389/fmars.2022.880550

Ortiz, J., J. Arístegui, J. Taucher, and U. Riebesell. 2022*b*. Artificial upwelling in singular and recurring mode: Consequences for net community production and metabolic balance. Front. Mar. Sci. **8**: 743105. doi:10.3389/fmars.2021.743105

Parada, A. E., D. M. Needham, and J. A. Fuhrman. 2016. Every base matters: Assessing small subunit rRNA primers for marine microbiomes with mock communities, time series and global field samples. Environ. Microbiol. **18**: 1403–1414. doi:10.1111/1462-2920.13023

Pohlert, T. 2022. PMCMRplus: Calculate pairwise multiple comparisons of mean rank sums extended. R package version 1.9.6 [accessed 2022 August 17]. Available from https://CRAN.R-project.org/package=PMCMRplus

Pontiller, B., and others. 2022. Rapid bacterioplankton transcription cascades regulate organic matter utilization during phytoplankton bloom progression in a coastal upwelling system. ISME J. **16**: 2360–2372. doi:10.1038/s41396-022-01273-0

R Core Team. 2021. R: A language and environment for statistical computing. R Foundation for Statistical Computing, [accessed 2021 November 01]. Available from https://www.R-project.org/

Reintjes, G., B. M. Fuchs, M. Scharfe, K. H. Wiltshire, R. Amann, and C. Arnosti. 2020. Short-term changes in polysaccharide utilization mechanisms of marine bacterioplankton during a spring phytoplankton bloom. Environ. Microbiol. **22**: 1884–1900. doi:10.1111/1462-2920.14971

Riebesell, U., and others. 2013. Technical note: A mobile sea-going mesocosm system—new opportunities for ocean change research. Biogeosciences **10**: 1835–1847. doi:10.5194/bg-10-1835-2013

Riemann, L., G. F. Steward, and F. Azam. 2000. Dynamics of bacterial community composition and activity during a mesocosm diatom bloom. Appl. Environ. Microbiol. **66**: 578–587. doi:10.1128/AEM.66.2.578-587.2000

Saba, G. K., D. K. Steinberg, and D. A. Bronk. 2011. The relative importance of sloppy feeding, excretion, and fecal pellet leaching in the release of dissolved carbon and nitrogen by *Acartia tonsa* copepods. J. Exp. Mar. Biol. Ecol. **404**: 47–56. doi:10.1016/j.jembe.2011.04.013

Salazar, G. 2022. EcolUtils: Utilities for community ecology analysis. R package version 0.1 [accessed 2022 July 14]. Available from https://github.com/GuillemSalazar/EcolUtils

Santana-Falcón, Y., X. A. Álvarez-Salgado, M. D. Pérez-Hernández, A. Hernández-Guerra, E. Mason, and J. Arístegui. 2017. Organic carbon budget for the eastern boundary of the North Atlantic subtropical gyre: Major role of DOC in mesopelagic respiration. Sci. Rep. **7**: 10129. doi:10.1038/s41598-017-10,974-y

Schwämmle, V., and O. N. Jensen. 2010. A simple and fast method to determine the parameters for fuzzy c-means cluster analysis. Bioinformatics **26**: 2841–2848. doi:10.1093/bioinformatics/btq534

Sidhu, C., and others. 2023. Dissolved storage glycans shaped the community composition of abundant bacterioplankton clades during a North Sea spring phytoplankton bloom. Microbiome **11**: 77. doi:10.1186/s40168-023-01517-x

Smith, D., and F. Azam. 1992. A simple, economical method for measuring bacterial protein synthesis rates in seawater using. Mar. Microb. Food Webs **6**: 107–114.

Sundby, S., K. F. Drinkwater, and O. S. Kjesbu. 2016. The North Atlantic spring-bloom system—where the changing climate meets the winter dark. Front. Mar. Sci. **3**: 28. doi:10.3389/fmars.2016.00028

Szabo, R. E., S. Pontrelli, J. Grilli, J. A. Schwartzman, S. Pollak, U. Sauer, and O. X. Cordero. 2022. Historical contingencies and phage induction diversify bacterioplankton communities at the microscale. Proc. Natl. Acad. Sci. **119**: e2117748119. doi:10.1073/pnas.2117748119

Taucher, J., and others. 2017. Influence of ocean acidification and deep water upwelling on oligotrophic plankton communities in the subtropical North Atlantic: Insights from

an in situ mesocosm study. Front. Mar. Sci. **4**: 85. doi:10.3389/fmars.2017.00085

Taucher, J., J. Arístegui, L. T. Bach, W. Guan, M. F. Montero, A. Nauendorf, E. P. Achterberg, and U. Riebesell. 2018. Response of subtropical phytoplankton communities to ocean acidification under oligotrophic conditions and during nutrient fertilization. Front. Mar. Sci. **5**: 330. doi:10.3389/fmars.2018.00330

Teeling, H., and others. 2012. Substrate-controlled succession of marine bacterioplankton populations induced by a phytoplankton bloom. Science **336**: 608–611. doi:10.1126/science.1218344

Zhou, J., G.-F. Chen, K.-Z. Ying, H. Jin, J.-T. Song, and Z.-H. Cai. 2019. Phycosphere microbial succession patterns and assembly mechanisms in a marine dinoflagellate bloom. Appl. Environ. Microbiol. **85**: e00349-19. doi:10.1128/AEM.00349-19

Acknowledgments

The authors thank the Plataforma Oceánica de Canarias (PLOCAN) for their support throughout the experiment, including the use of their facilities and their assistance during the sampling of the mesocosms. The authors thank the whole KOSMOS team (GEOMAR) and the Biological Oceanography Group of the ULPGC for their effort in organizing and carrying out the experiment. Thanks also go to Irene Forn (ICM, CSIC) for her help during the processing of BONCAT samples and the subsequent image acquisition. This study is a contribution to the Ocean Artificial Upwelling project (Ocean artUp), funded by an Advanced Grant of the European Research Council (No. 695094) awarded to UR. Additional support was provided through projects FLUXES (CTM2015-69392-C3-1-R) and e-IMPACT (PID2019-109084RB-C21) funded by the Spanish National Science Plan. MGL was supported by the Ministerio de Universidades, Gobierno de España (FPU17-01435) during their PhD. MS was supported by the Project MIAU (RTI2018-101025-B-I00), MICOLOR (PID2021-125469NB-C31), the "Severo Ochoa Centre of Excellence" accreditation (CEX2019-000928-S), and by a Viera y Clavijo contract funded by the ACIISI and the ULPGC. JA was supported by a Helmholtz International Fellow Award, 2015 (Helmholtz Association, Germany) and by the United States National Science Foundation grant OCE-1840868 to the Scientific Committee on Oceanic Research (SCOR, United States) WG 155.

Conflict of Interest

None declared.

Submitted 29 May 2024
Revised 21 September 2024
Accepted 05 December 2024

Associate Editor: Laura Bristow